Ligand-specific allosteric coupling controls G protein-coupled receptor signaling

Janine Holze[1,#], Marcel Bermudez[2,#], Eva Marie Pfeil[3], Michael Kauk[4], Theresa Bödefeld[1], Matthias Irmen[1], Carlo Matera[5], Clelia Dallanoce[5], Marco De Amici[5], Ulrike Holzgrabe[6], Gabriele Maria König[7], Christian Tränkle[1], Gerhard Wolber[2], Ramona Schrage[1], Klaus Mohr[1], Carsten Hoffmann[4], Evi Kostenis[3], and Andreas Bock[1,8]**

[1]Pharmacology and Toxicology Section, Institute of Pharmacy, University of Bonn, Bonn, Germany

[2]Institute of Pharmacy, Freie Universität Berlin, Berlin, Germany

[3]Molecular, Cellular and Pharmacobiology Section, Institute for Pharmaceutical Biology, University of Bonn, Bonn, Germany

[4]Institute for Molecular Cell Biology, CMB—Center for Molecular Biomedicine, University Hospital Jena, Friedrich Schiller University Jena, Jena, Germany

[5]Department of Pharmaceutical Sciences, University of Milan, Milan, Italy

[6]Department of Pharmaceutical and Medical Chemistry, Institute of Pharmacy, University of Würzburg, Würzburg, Germany

[7]Institute for Pharmaceutical Biology, University of Bonn, Bonn, Germany

[8]Max-Delbrueck-Center for Molecular Medicine in the Helmholtz Association, Berlin, Germany

# These authors contributed equally to this work.

* Correspondence should be addressed to Andreas Bock (andreas.bock@mdc-berlin.de) or Evi Kostenis (kostenis@uni-bonn.de).

ABSTRACT:

Allosteric coupling describes a reciprocal process whereby G protein-coupled receptors (GPCRs) relay ligand-induced conformational changes from the extracellular binding pocket to the intracellular signaling surface. Therefore, GPCR activation is sensitive to both the type of extracellular ligand and intracellular signaling protein. We hypothesized that ligand-specific allosteric coupling may result in preferential (i.e. biased) engagement of downstream effectors. However, the structural basis underlying ligand-dependent control of this essential allosteric mechanism is poorly understood. Here, we show that two sets of extended muscarinic acetylcholine receptor M_1 agonists, which only differ in linker length, progressively constrain receptor signaling. We demonstrate that stepwise shortening of their chemical linker gradually hampers binding pocket closure resulting in divergent coupling to distinct G-protein families. Our data provide an experimental strategy for the design of ligands with selective G-protein recognition and reveal a potentially general mechanism of ligand-specific allosteric coupling.

KEYWORDS:

G protein-coupled receptors, allosteric coupling, bitopic ligands, muscarinic receptors, biased signaling, G-protein selectivity

G protein-coupled receptors (GPCRs) are ubiquitous membrane proteins which sense a myriad of extracellular stimuli such as neurotransmitters and hormones among many others, and transmit them to the cell interior mainly through activation of heterotrimeric G protein-signaling cascades[1]. Given their abundance and ubiquitous expression, GPCRs modulate almost every physiological process and often play pivotal roles in disease, rationalizing why this protein family is among the most popular drug targets[2]. Individual GPCRs frequently activate multiple downstream second messenger and/or protein kinase cascades after engagement of one or more G proteins from one subfamily or, alternatively, multiple G proteins from the four distinct families[3]. The past decade has witnessed an ever increasing number of studies to exploit this signaling multiplicity for the possibility of designing drugs with greater specificity and fewer side effects. In line with this, so-called biased ligands have been developed, which preferentially activate only a subset of all possible GPCR signaling pathways, unlike their unbiased counterparts[4, 5]. From a drug discovery point of view, functionally selective ligands are particularly interesting for their potential to promote therapeutically desired signaling while simultaneously sparing other, potentially harmful signaling routes. However, the structural basis of how biased ligands lead to selective GPCR signaling is only beginning to be understood and it is largely unknown how such ligands need to be designed.

Recent crystal and cryo-EM structures of GPCRs have revealed in atomic detail that agonist binding to GPCRs results in large-scale conformational changes in the receptor protein which allow intracellular coupling to signaling proteins. Most prominently, receptor activation requires an outward movement of the intracellular part of transmembrane domain 6 facilitating G-protein binding. Reciprocally, this intracellular outward movement and G-protein coupling is accompanied by an inward movement of extracellular parts of TM 5 and 7 and rearrangement of extracellular loops resulting in a contraction of the ligand binding pocket[1]. Biophysical and

biochemical experiments have shown that intracellular G-protein binding traps the agonist in the extracellular ligand binding pocket[6, 7]. This mechanism of GPCR activation occurs via a series of reciprocal conformational changes between the ligand and the G protein-binding site, and is referred to as allosteric coupling. Allosteric coupling forms the structural basis for the well-described pharmacological phenomenon that G-protein binding to GPCRs increases agonist, but not antagonist, affinity and *vice versa*[8]. It is intriguing to speculate that binding of different intracellular effectors might be inseparably linked to divergent conformational changes on the extracellular receptor side, for instance to different degrees of binding pocket closure[9]. In favor of this hypothesis, recent structural evidence from the muscarinic M_2 receptor[10, 11] and the β_1 adrenergic receptor[12] suggests that extracellular conformational changes resulting from G-protein coupling are distinct from those induced by β-arrestin binding. However, it is entirely unknown whether divergent allosteric coupling determines preference amongst G-protein families, thereby modulating G-protein selectivity, and whether this can be specifically tuned by ligands.

Here, using the muscarinic acetylcholine receptor M_1 (M_1R) as a model, we directly probed the impact of ligand-specific allosteric coupling on the receptor's preference for G proteins ($G_{q/11}$, G_s, $G_{i/o}$) with two sets of extended, bitopic agonists which only differ in the length of the linker connecting an orthosteric agonist moiety to a negative allosteric modulator moiety. Gradual shortening of the linker resulted in progressive loss of the receptor's ability to couple to certain G proteins ($G_{i/o}$ and G_s) while maintaining robust coupling to $G_{q/11}$. Molecular modeling studies suggested that the bitopic ligands gradually inhibit ligand binding pocket closure in a manner directly related to their linker length. Using a biosensor for M_1R activation based on Foerster resonance energy transfer (FRET), we demonstrate that intracellular conformational changes of the receptor at the G protein-coupling interface gradually depended on the linker length of the bitopic

ligands. Our data illustrate that ligand-dependent allosteric coupling allows selective G-protein signaling.

RESULTS AND DISCUSSION

The muscarinic M_1 receptor (M_1R) is known to couple to several G-protein families[13]. In addition to its cognate $G_{q/11}$-protein family, M_1Rs promote signaling through both G_s and $G_{i/o}$ proteins. To quantitatively assess the G protein-coupling profile of M_1Rs stably expressed in CHO cells (CHO-M_1) at endogenous G-protein expression, we performed second messenger assays (IP1 and cAMP) as well as GTPγS binding in intact CHO-M_1 cells and membranes thereof, respectively (**Figure 1**). The endogenous neurotransmitter acetylcholine (ACh) and iperoxo served as orthosteric agonists to assess the coupling of M_1R to $G_{q/11}$, G_s, and $G_{i/o}$. Both agonists evoked potent and efficacious increases of total cellular IP1 and cAMP concentration, and induced robust [^{35}S]GTPγS binding (**Figure 1**). Iperoxo displayed an approximately 100-fold higher potency than ACh in all three assays while it was equally efficacious as deduced from equivalent Emax values. As second messenger levels in cells are well known to result from a complex interplay between different G-protein families and, therefore, do not serve as unambiguous indicators for specific G-protein recognition, we used G protein-selective inhibitors, rather than a GTPγS immunoprecipitation assay[14], to isolate and dissect the respective M_1R signaling pathways. Pretreatment of cells with the $G_{q/11}$-specific inhibitor FR900359 (FR) abolished both ACh- (**Figure 1A and 1B**) and iperoxo-stimulated (**Figure 1A and 1C**) IP1 accumulation, indicating that this response is exclusively dependent on M_1R-mediated activation of $G_{q/11}$ proteins. M_1R-induced cAMP accumulation (**Figure 1D**) was also reduced, by more than 50 percent, in the presence of FR, indicating a strong $G_{q/11}$ component in the signaling network that controls cAMP production (**Figure 1E and 1F**). Co-treatment of CHO-M_1 cells with FR and pertussis toxin (PTX) to inhibit $G_{q/11}$ and $G_{i/o}$ proteins,

reversed the cAMP lowering effects of FR for both agonists and unmasked the inhibitory effect of $G_{i/o}$ proteins on cAMP accumulation (**Figure 1E and 1F**). This cAMP response, achieved after pharmacological silencing of $G_{i/o}$ and $G_{q/11}$ proteins, represents the M_1R's ability to directly activate G_s signaling. Thus, while our data indicate that cAMP accumulation is a highly integrated response that is orchestrated by three major G-protein families, combined pretreatment of CHO-M_1 cells with PTX and FR does allow to single out endogenous M_1R-mediated G_s signaling without the confounding input of $G_{i/o}$ and $G_{q/11}$ proteins. Binding of [^{35}S]GTPγS is another widely used method to unveil receptor-stimulated activation of endogenous G proteins. This method has proven particularly useful to quantify receptor-mediated GTPγS loading onto $G_{i/o}$ proteins but is, in principle, not restricted to the detection of receptor $G_{i/o}$ interaction. Iperoxo and ACh both stimulated M_1R-mediated [^{35}S]GTPγS binding (**Figure 1G**), and these responses reflected engagement of $G_{i/o}$ and $G_{q/11}$ proteins as evidenced by their significant reduction when membranes were collected from cells after pre-treatment with PTX or FR (**Figure 1H and 1I**). Combined pretreatment with both inhibitors largely eliminated ACh (**Figure 1H**) and iperoxo-stimulated (**Figure 1I**) [^{35}S]GTPγS binding, yet PTX effects appeared more pronounced than those observed with FR. Therefore, we inferred that [^{35}S]GTPγS loading of CHO-M_1 membranes preferentially reported on $G_{i/o}$-activation.

Bitopic ligands are compounds which possess two building blocks that target two distinct binding sites at one receptor protomer, i.e. the orthosteric and a second topographically distinct, allosteric binding site[15]. We here use two sets of bitopic ligands which are composed of the orthosteric agonist iperoxo and two negative allosteric modulators covalently linked by methylene linkers of varying length (**Figure 2**). The *phth*-series of ligands contains iperoxo and a fragment of the allosteric modulator W84 connected by 6 (iper-6-phth), 7 (iper-7-phth), or 8 methylene groups (iper-8-phth). The *naph*-series follows the same ligand design principle by using a fragment of the

allosteric modulator naphmethonium (i.e. iper-6-naph, iper-7-naph, iper-8-naph). Previously, both series have been characterized extensively at the muscarinic M_2 receptor[16]. Radioligand binding experiments (**Supporting Methods**) using the orthosteric antagonist [^{3}H]NMS as a tracer demonstrated that all bitopic ligands are able to bind to both the allosteric binding site, as derived from dissociation binding (**Figure S1**), and the orthosteric binding site, as inferred from equilibrium binding (**Figure S2**). Whereas ligand affinities for the allosteric binding site within one ligand series were highly similar (**Table S1**), ligand affinities for the orthosteric binding site depended on linker length, whereby increasing linker length correlated with increased ligand affinity (**Table S2**). Therefore, we reasoned that the three bitopic ligands within a series adopted the same binding mode in the orthosteric site driven by iperoxo's high affinity. In consequence, a set of bitopic ligands – which only differ in linker length – may qualify to precisely probe the impact of ligand binding pocket closure, and thereby altered allosteric coupling, on GPCR signaling with sub-nanometer precision. While all bitopic ligands of the *phth*-series promoted $G_{q/11}$-protein signaling, iper-6-phth conferred partial activation only (**Figure 2B**). However, when G_s-mediated cAMP accumulation was quantified as receptor signaling output, we found agonism across the full efficacy range with iper-8-phth being fully active, iper-7-phth partly active, and iper-6-phth completely incompetent to evoke elevation of cAMP above basal levels (**Figure 2D**). However, when cAMP production was measured in the absence of PTX and FR (**Figure S3**), iper-6-phth did augment this second messenger, corroborating its productive $G_{q/11}$-protein coupling (**Figure 2B**), and attesting to the validity of our cAMP assay regime to single out pathways by means of inhibitor compounds. M_1R-mediated $G_{i/o}$ protein activation was only induced by iper-8-phth. Iper-7-phth and iper-6-phth both failed to promote effective $M_1R/G_{i/o}$-coupling (**Figure 2F**). From these data we concluded that gradual shortening of the linker of bitopic ligands results in progressive loss of G protein-signaling capacity. While the most extended bitopic agonist iper-8-

phth was capable of stimulating all three G-protein families, iper-7-phth activated $G_{q/11}$ and G_s proteins, while iper-6-phth promoted signaling through $G_{q/11}$ only.

The second series of bitopic ligands (i.e. the *naph*-series) contains an allosteric modulator which differs from the *phth* derivative mainly in two aspects: *naph* has a larger size and is characterized by a branched aliphatic linker (**Figure 2A**). We hypothesized that the *naph*-series would more severely interfere with M_1R G-protein signaling. Indeed, while the extended bitopic ligands iper-7-naph and iper-8-naph promoted $G_{q/11}$-protein signaling, iper-6-naph failed to activate this signaling route (**Figure 2C**), in stark contrast to iper-6-phth (**Figure 2B**). In addition, none of the *naph*-based bitopic ligands was able to stimulate G_s (**Figure 2E**) and $G_{i/o}$ signaling (**Figure 2G**). Again, iper-7-naph and iper-8-naph increased cAMP levels when PTX and FR were absent (**Figure S3**). Interestingly, iper-6-naph, which is devoid of intrinsic activity on any of the tested G proteins, strongly inhibited ACh-stimulated IP1 and cAMP accumulation, as well as [^{35}S]GTPγS binding (**Figure S4**). In line with this finding, iper-6-phth, which exclusively activated $G_{q/11}$ proteins, completely abolished ACh-induced [^{35}S]GTPγS binding and partially inhibited cAMP accumulation (**Figure S4**). Moreover, iper-7-phth, a bitopic agonist which does not stimulate M_1R $G_{i/o}$ coupling (**Figure 2F**), antagonized ACh-induced $G_{i/o}$ activation (**Figure S4**). These data suggest that different G proteins display distinct sensitivities towards M_1R activation by the above set of extended ligands. Whereas $G_{q/11}$ coupling is preserved by almost all bitopic ligands (except iper-6-naph), G_s signaling is only promoted by two extended members of the *phth*-series (i.e. iper-7-phth and iper-8-phth), while $G_{i/o}$ activation is particularly susceptible to bitopic ligand structure (only iper-8-phth showed weak $M_1R/G_{i/o}$ coupling). These data reveal a clear hierarchy of G-protein recognition by M_1Rs with the cognate $G_{q/11}$ protein tolerating most bitopic ligands, followed by G_s and $G_{i/o}$. Strikingly, only very subtle, i.e. sub-nanometer, changes in bitopic ligand length had profound effects on the ability of M_1Rs to couple to different G-protein families.

To gain mechanistic insight into the structural basis underlying G protein-coupling selectivity of bitopic ligands, we performed binding mode investigations by molecular docking and all-atom molecular dynamics (MD) simulations on a microsecond time scale. We used a previously developed M_1R model which is almost equivalent to the recent M_1R cryo-EM structure (**Figure S5**). Initial docking results suggest that the iperoxo moiety, due to its high affinity (**Figure S2**), binds in a nearly identical way compared to iperoxo itself and serves as a structural anchor for the binding mode of bitopic ligands (**Figure 3A-D**), similar to previously reported data from bitopic ligands for the M_2 receptor[17]. This 'affinity-anchoring' ensures that bitopic ligands which only differ in linker length results in stepwise interference with extracellular regions of the receptor that have been shown to contract upon receptor activation (**Figure S6**). MD simulations confirm these binding modes and provide insights into conformational dynamics of extracellular parts of the ligand binding pocket. Iperoxo binding results in full contraction of the extracellular parts of the ligand binding pocket. In contrast, the bitopic ligands of the *phth*-series bind in a way that sterically hinders binding pocket closure. Interestingly, the degree of conformational interference appears to depend on linker length and thereby the position of the allosteric building block (**Figure 3E-H**). Since the *phth*-moiety of iper-6-phth is positioned more deeply in the receptor core (closer to the orthosteric binding site), it hampers binding pocket closure more severely resulting in a more open extracellular conformation (**Figure 3H**). Elongation of the linker by additional methylene groups allowed sub-nanometer control of the position of the allosteric building block and thereby gradually reduces the conformational interference with binding pocket closure, eventually resulting in a greater G protein-coupling capability (**Figure 2**). The alpha carbon distance between $Y179^{ECL2}$ and $T389^{6.59}$ illustrates temporal dynamics of how bitopic ligands interfere with binding pocket closure (**Figure 3I-J**).

Docking and molecular dynamics simulations demonstrate that bitopic ligands adopted binding poses that interfere with closure of the binding pocket in a linker-length dependent manner. It is likely that interference with binding pocket closure impacts the intracellular G protein-binding interface through allosteric coupling and, thus, may be the molecular basis for the experimentally observed G protein-coupling profiles of bitopic ligands. To test this hypothesis, we performed single-cell FRET measurements and investigated whether ligand-dependent interference with binding pocket closure translated into altered receptor conformations at the intracellular G protein-coupling interface. We used a previously characterized M_1R-FRET sensor that reports on agonist-mediated receptor activation with an increase in FRET ratio between the C-terminal donor CFP and a FlAsH acceptor incorporated in intracellular loop 3[18] (**Figure 4A**). Superfusion of HEK293 cells stably expressing the M_1R-FRET sensor with iperoxo led to a rapid increase in FRET ratio which was reversible upon ligand wash-out (**Figure 4B**). Superfusion of sensor expressing cells with bitopic ligands from the *phth*-series induced robust, albeit small, increases in FRET (**Figure 4B-D**). Interestingly, the maximal FRET change induced by bitopic ligands appeared to correlate with linker length (**Figure 4F**). The bitopic ligand with the longest linker, iper-8-phth, (**Figure 4B**), triggered a significantly larger FRET change than the shorter derivatives iper-7-phth (**Figure 4C**) and iper-6-phth (**Figure 4D**). Iper-6-naph, a bitopic ligand with a branched and larger allosteric moiety, which was found to be incompatible with the active M_1R conformation (**Figure S6C**), failed to induce M_1R conformational changes (**Figure 4E**). However, and entirely in line with our proposed concept of allosteric coupling, mutational removal of the steric clash ($W400^{7.35}A$) was sufficient to confer some degree of agonist activity onto iper-6-naph (**Figure S7**).

In summary, our data demonstrate that pleiotropic G-protein coupling of GPCRs requires orthosteric activation by agonists which is accompanied by pronounced extracellular conformational changes of the receptor, resulting in closure of the ligand binding pocket from the

extracellular space. Designed bitopic ligands incorporating parts which bind to epitopes of the extracellular receptor domains and only differ in molecule length function as atomic rulers to interfere with ligand binding pocket closure at sub-nanometer precision. We propose a ligand-dependent allosteric coupling mechanism which links the degree of extracellular binding pocket closure to the extent of intracellular conformational changes at the G protein-binding interface as revealed by FRET measurements. Albeit future studies will need to map and integrate receptor conformational changes at different positions, our data strongly suggest that a more closed ligand binding pocket is accompanied by larger receptor conformational changes at the G protein-binding interface through an allosteric coupling mechanism.

Ligand-dependent modulation of this mechanism allows generation of pathway-selective, i.e. biased, ligands. Interestingly, at related GPCRs (muscarinic M_2, dopamine D_2, serotonin 5-HT_2B) several studies have reported that ligands with an 'extended binding mode' are biased and that, structurally, bias is encoded in parts of the ligand that target the extracellular receptor domains[9, 16, 19, 20]. The bitopic ligands studied here can be considered as a particular example for 'extended ligands' where the extended part constitutes an allosteric modulator. Therefore, we suggest that ligand-specific allosteric coupling by extended (bitopic) ligands constitutes a general mechanism of how GPCRs can be steered into specific signaling pathways. We propose that bitopic ligands or, more generally, 'extended ligands' provide excellent tools to exert control over G-protein recognition to finetune the signaling range of GPCRs with unprecedented precision.

MATERIALS AND METHODS:

Cell culture:

Chinese hamster ovary (CHO) cells stably expressing the human muscarinic M_1 acetylcholine receptor (CHO-M_1) or the mutant $W400^{7.35}A$ were cultured in Ham's nutrient mixture F-12 supplemented with 10% (v/v) fetal calf serum (FCS), 100 U mL^{-1} penicillin, 100 µg mL^{-1} streptomycin, 2 mM L-glutamine, and 0.2 mg mL^{-1} G418. HEK293 cells stably expressing the M1-I3N-CFP receptor FRET sensor were maintained in DMEM with 4.5 g L^{-1} glucose, 10% (v/v) FCS, 100 U mL^{-1} penicillin, 100 µg mL^{-1} streptomycin, 2 mM L-glutamine and 0.2 mg mL^{-1} G418. All cell lines were cultured at 37 °C in a humidified 7% CO_2 atmosphere and were routinely passaged every two to three days.

IP1 accumulation and cAMP accumulation assays:

M_1R-mediated total IP1 and cAMP accumulation were detected using the IP-One HTRF® assay kit and HTRF-cAMP dynamic kit (Cisbio, France), respectively, according to the manufacturer's instructions. 50,000 cells/well (for IP1 assays) or 1,000 cells/well (for cAMP assays) were seeded in 384 well microtiter plates. Under some conditions, cells were pretreated with 50 ng/mL PTX overnight and/or preincubated with 1 µM FR900359 for 1 h. For experiments in antagonist mode, cells were pre-incubated with antagonist for 1 h prior to agonist stimulation. 30 min after agonist stimulation, IP1 and cAMP were detected as HTRF ratios using a Mithras LB 940 reader (Berthold Technologies, Germany).

[^{35}S]GTPγS binding assays:

40 µg/mL membranes were incubated with increasing concentrations of test compounds and 0.07 nM [^{35}S]GTPγS in HEPES buffer for 60 min at 30°C. 1 µM GDP was added to decrease the basal

turnover rate of endogenous G proteins. In the case of $G_{q/11}$ protein inhibition, membranes were pre-incubated with FR900359 (1 µM) for 1 h at 30 °C. For the inhibition of $G_{i/o}$ proteins, PTX pre-incubated membranes were used (100 ng/mL PTX added 24 h before membrane preparation). Experiments were terminated by rapid vacuum filtration. After melting scintillation wax, filter-bound radioactivity was quantified by solid scintillation counting.

Docking and molecular dynamics simulations:

The inactive M_1 receptor crystal structure (PDB: 5CXV[21]), the active M_1 receptor cryo-EM structure (PDB: 6OIJ[10]) and active-like homology models of the M_1 receptor[22] were used for molecular docking with the CCDCs software GOLD version 5.2. Default settings were applied for receptor-ligand docking with all residues of the receptor core region and the extracellular regions defined as potential binding site and using GoldScore as primary scoring function. Subsequently, molecular dynamics simulations were carried out in triplicates on a local graphics cards cluster (Nvidia rtx-2080-ti at Molecular Design Lab, Freie Universität Berlin) with Desmond 2018.3 following the previously published procedure[23] and a simulation time of 1 µs each (further details in **Figure S8**). MD trajectories were analyzed with the software VMD 1.9.3 and LigandScout 4.4[24].

Single-cell FRET measurements:

FlAsH labeling and FRET measurements were conducted exactly as described previously[18].

Data analysis:

Nonlinear regression analysis was performed using GraphPad Prism 8 (GraphPad Software, San Diego, CA). [^{35}S]GTPγS-binding, IP1- and cAMP-accumulation data were baseline-corrected by subtracting the value of buffer-stimulated cells and normalized to the maximum effect of ACh or

iperoxo. Concentration-effect-curves were fitted by a four-parameter-logistic function yielding parameter values for a ligand´s potency (pEC_{50}) and maximum effect (E_{max}).

Statistical analysis:

To compare two means, statistical significance was based on a Student´s *t*-test with $P < 0.05$, to compare one mean to a fixed value, statistical significance was based on a one-sample t-test with $P < 0.05$. Comparisons of groups were performed using one-way-ANOVA analysis with a Tukey-Kramer Post-Test.

AUTHOR CONTRIBUTIONS:

R.S., K.M., E.K. and A.B. conceived of the project. J.H., M.B., E.M.P., M.K., T.B., and M.I. performed experiments and analyzed data with support from C.T., G.W., R.S., K.M., C.H., E.K., and A.B. C.M., C.D., M.D.A., and U.H designed and synthesized all bitopic ligands. G.M.K. isolated and provided FR900359. J.H., M.B., and E.M.P. prepared figures. E.K. and A.B. oversaw overall research and wrote the paper with input from all authors.

NOTES

The authors declare no competing financial interest.

ACKNOWLEDGEMENTS

We thank Arthur Christopoulos (Monash University, Melbourne, Australia) for providing the stable CHO-M1 W400$^{7.35}$A cell line and Iris Jusen and Dieter Baumert (both University of Bonn) for technical assistance. M.B. acknowledges funding by the Deutsche Forschungsgemeinschaft (German Research Foundation, project number 407626949) and support by the Joachim Herz Stiftung. E.P. is funded by the Deutsche Forschungsgemeinschaft (DFG, German Research Foundation)-214362475/GRK1873/2. E.K. and G.M.K. gratefully acknowledge support of this work by the DFG-funded Research Unit FOR2372 with the grants KO 1582/10-1 and KO 1582/10-2 (to E.K), as well as KO 902/17-1 and KO 902/17-2 (to G.M.K.). A.B. acknowledges funding by the Deutsche Forschungsgemeinschaft (DFG, German Research Foundation) through SFB1423, project number 421152132, subproject C05.

SUPPORTING INFORMATION

Supporting Methods: Radioligand binding experiments. **Figure S1**: [^{3}H]NMS dissociation binding; **Figure S2**: Equilibrium binding of iperoxo and bitopic ligands; **Figure S3**: cAMP assays without PTX and FR; **Figure S4**: Bitopic ligands in antagonist mode; **Figure S5**: Structural comparison M_1R model vs. cryo-EM structure; **Figure S6**: Binding modes of bitopic ligands; **Figure S7**: Effect of iper-6-naph on IP1 production at M1 W400$^{7.35}$A mutant receptors; **Figure S8**: Extended characterization of MD simulation data; **Table S1**: pEC50, diss values of bitopic ligands; **Table S2**: Affinities of bitopic ligands for M_1 receptors; **Supporting References**.

REFERENCES

1. Weis, W. I.; Kobilka, B. K., The Molecular Basis of G Protein-Coupled Receptor Activation. *Annu Rev Biochem* **2018,** *87*, 897-919.

2. Hauser, A. S.; Attwood, M. M.; Rask-Andersen, M.; Schioth, H. B.; Gloriam, D. E., Trends in GPCR drug discovery: new agents, targets and indications. *Nat Rev Drug Discov* **2017,** *16* (12), 829-842.

3. Oldham, W. M.; Hamm, H. E., Heterotrimeric G protein activation by G-protein-coupled receptors. *Nat Rev Mol Cell Biol* **2008,** *9* (1), 60-71.

4. Smith, J. S.; Lefkowitz, R. J.; Rajagopal, S., Biased signalling: from simple switches to allosteric microprocessors. *Nat Rev Drug Discov* **2018,** *17* (4), 243-260.

5. Wootten, D.; Christopoulos, A.; Marti-Solano, M.; Babu, M. M.; Sexton, P. M., Mechanisms of signalling and biased agonism in G protein-coupled receptors. *Nat Rev Mol Cell Biol* **2018,** *19* (10), 638-653.

6. Kruse, A. C.; Ring, A. M.; Manglik, A.; Hu, J.; Hu, K.; Eitel, K.; Hubner, H.; Pardon, E.; Valant, C.; Sexton, P. M.; Christopoulos, A.; Felder, C. C.; Gmeiner, P.; Steyaert, J.; Weis, W. I.; Garcia, K. C.; Wess, J.; Kobilka, B. K., Activation and allosteric modulation of a muscarinic acetylcholine receptor. *Nature* **2013,** *504* (7478), 101-6.

7. DeVree, B. T.; Mahoney, J. P.; Velez-Ruiz, G. A.; Rasmussen, S. G.; Kuszak, A. J.; Edwald, E.; Fung, J. J.; Manglik, A.; Masureel, M.; Du, Y.; Matt, R. A.; Pardon, E.; Steyaert, J.; Kobilka, B. K.; Sunahara, R. K., Allosteric coupling from G protein to the agonist-binding pocket in GPCRs. *Nature* **2016,** *535* (7610), 182-6.

8. Kent, R. S.; De Lean, A.; Lefkowitz, R. J., A quantitative analysis of beta-adrenergic receptor interactions: resolution of high and low affinity states of the receptor by computer modeling of ligand binding data. *Mol Pharmacol* **1980,** *17* (1), 14-23.

9. Bermudez, M.; Bock, A., Does Divergent Binding Pocket Closure Drive Ligand Bias for Class A GPCRs? *Trends Pharmacol Sci* **2019,** *40* (4), 236-239.

10. Maeda, S.; Qu, Q.; Robertson, M. J.; Skiniotis, G.; Kobilka, B. K., Structures of the M1 and M2 muscarinic acetylcholine receptor/G-protein complexes. *Science* **2019,** *364* (6440), 552-557.

11. Staus, D. P.; Hu, H.; Robertson, M. J.; Kleinhenz, A. L. W.; Wingler, L. M.; Capel, W. D.; Latorraca, N. R.; Lefkowitz, R. J.; Skiniotis, G., Structure of the M2 muscarinic receptor-beta-arrestin complex in a lipid nanodisc. *Nature* **2020,** *579* (7798), 297-302.

12. Lee, Y.; Warne, T.; Nehme, R.; Pandey, S.; Dwivedi-Agnihotri, H.; Chaturvedi, M.; Edwards, P. C.; Garcia-Nafria, J.; Leslie, A. G. W.; Shukla, A. K.; Tate, C. G., Molecular basis of beta-arrestin coupling to formoterol-bound beta1-adrenoceptor. *Nature* **2020,** *583* (7818), 862-866.

13. Inoue, A.; Raimondi, F.; Kadji, F. M. N.; Singh, G.; Kishi, T.; Uwamizu, A.; Ono, Y.; Shinjo, Y.; Ishida, S.; Arang, N.; Kawakami, K.; Gutkind, J. S.; Aoki, J.; Russell, R. B., Illuminating G-Protein-Coupling Selectivity of GPCRs. *Cell* **2019,** *177* (7), 1933-1947 e25.

14. Harrison, C.; Traynor, J. R., The [35S]GTPgammaS binding assay: approaches and applications in pharmacology. *Life Sci* **2003,** *74* (4), 489-508.

15. Bock, A.; Schrage, R.; Mohr, K., Allosteric modulators targeting CNS muscarinic receptors. *Neuropharmacology* **2018,** *136* (Pt C), 427-437.

16. Bock, A.; Merten, N.; Schrage, R.; Dallanoce, C.; Batz, J.; Klockner, J.; Schmitz, J.; Matera, C.; Simon, K.; Kebig, A.; Peters, L.; Muller, A.; Schrobang-Ley, J.; Trankle, C.; Hoffmann, C.; De Amici, M.; Holzgrabe, U.; Kostenis, E.; Mohr, K., The allosteric vestibule of a seven transmembrane helical receptor controls G-protein coupling. *Nat Commun* **2012,** *3*, 1044.

17. Bermudez, M.; Bock, A.; Krebs, F.; Holzgrabe, U.; Mohr, K.; Lohse, M. J.; Wolber, G., Ligand-Specific Restriction of Extracellular Conformational Dynamics Constrains Signaling of the M2 Muscarinic Receptor. *ACS Chem Biol* **2017,** *12* (7), 1743-1748.

18. Messerer, R.; Kauk, M.; Volpato, D.; Alonso Canizal, M. C.; Klockner, J.; Zabel, U.; Nuber, S.; Hoffmann, C.; Holzgrabe, U., FRET Studies of Quinolone-Based Bitopic Ligands and Their Structural Analogues at the Muscarinic M1 Receptor. *ACS Chem Biol* **2017,** *12* (3), 833-843.

19. Wacker, D.; Wang, S.; McCorvy, J. D.; Betz, R. M.; Venkatakrishnan, A. J.; Levit, A.; Lansu, K.; Schools, Z. L.; Che, T.; Nichols, D. E.; Shoichet, B. K.; Dror, R. O.; Roth, B. L., Crystal Structure of an LSD-Bound Human Serotonin Receptor. *Cell* **2017,** *168* (3), 377-389 e12.

20. McCorvy, J. D.; Butler, K. V.; Kelly, B.; Rechsteiner, K.; Karpiak, J.; Betz, R. M.; Kormos, B. L.; Shoichet, B. K.; Dror, R. O.; Jin, J.; Roth, B. L., Structure-inspired design of beta-arrestin-biased ligands for aminergic GPCRs. *Nat Chem Biol* **2018,** *14* (2), 126-134.

21. Thal, D. M.; Sun, B.; Feng, D.; Nawaratne, V.; Leach, K.; Felder, C. C.; Bures, M. G.; Evans, D. A.; Weis, W. I.; Bachhawat, P.; Kobilka, T. S.; Sexton, P. M.; Kobilka, B. K.; Christopoulos, A., Crystal structures of the M1 and M4 muscarinic acetylcholine receptors. *Nature* **2016,** *531* (7594), 335-40.

22. Bermudez, M.; Rakers, C.; Wolber, G., Structural Characteristics of the Allosteric Binding Site Represent a Key to Subtype Selective Modulators of Muscarinic Acetylcholine Receptors. *Mol Inform* **2015,** *34* (8), 526-30.

23. Bock, A.; Bermudez, M.; Krebs, F.; Matera, C.; Chirinda, B.; Sydow, D.; Dallanoce, C.; Holzgrabe, U.; De Amici, M.; Lohse, M. J.; Wolber, G.; Mohr, K., Ligand Binding Ensembles Determine Graded Agonist Efficacies at a G Protein-coupled Receptor. *J Biol Chem* **2016,** *291* (31), 16375-89.

24. Wolber, G.; Langer, T., LigandScout: 3-D pharmacophores derived from protein-bound ligands and their use as virtual screening filters. *J Chem Inf Model* **2005,** *45* (1), 160-9.

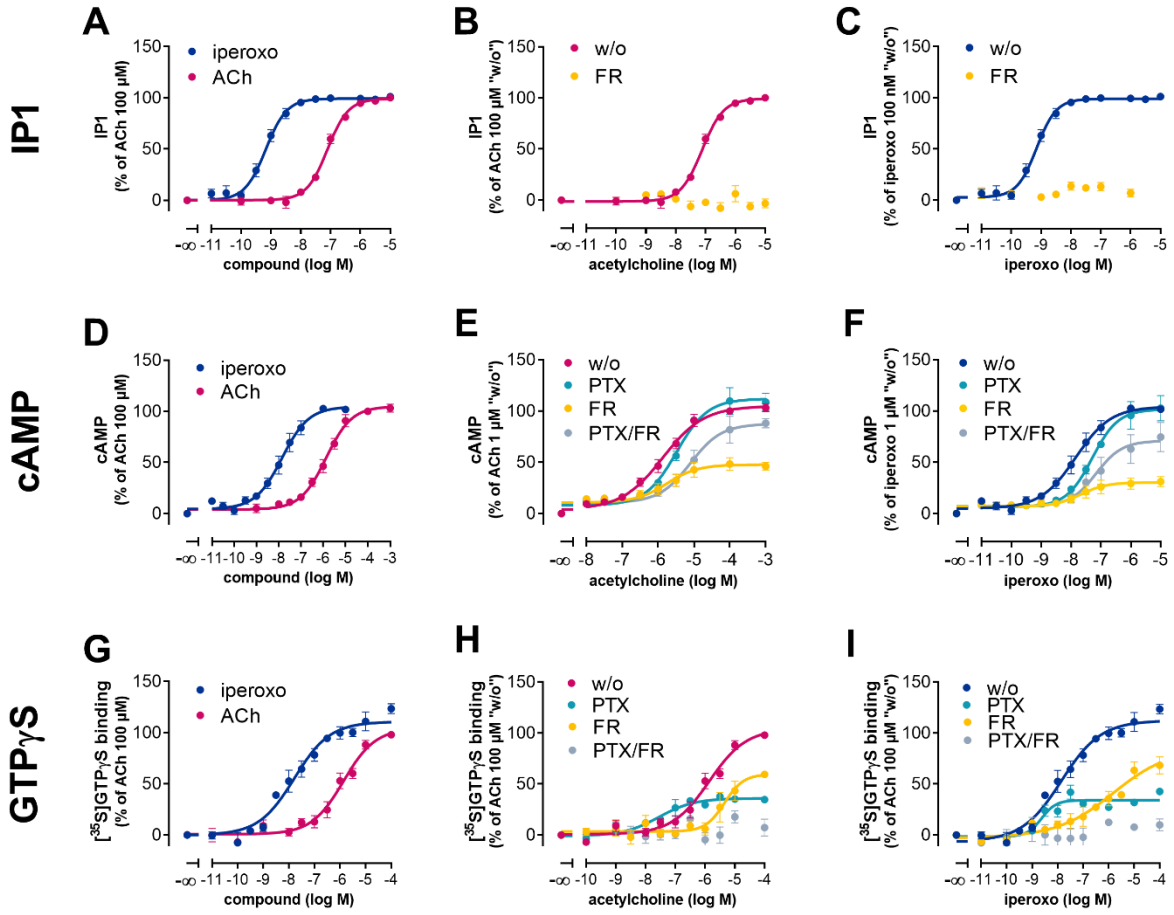

Figure 1: The M_1 receptor couples to three major G-protein families in CHO cells. (**A-I**) Concentration-response-curves of ACh- and iperoxo-stimulated IP1 production (**A-C**), cAMP accumulation (**D-F**), and [^{35}S]GTPγS binding (**G-I**) in CHO-M_1 cells or membranes (**G-I**). M_1R-mediated IP1 accumulation is exclusively mediated by $G\alpha_{q/11}$ as pretreatment with the $G\alpha_{q/11}$ specific inhibitor FR900359 (1 µM) abolished the response (**B, C**). cAMP accumulation is an integrated response with contribution from $G\alpha_{q/11}$, $G\alpha_{i/o}$, $G\alpha_s$. Inhibition of $G\alpha_{q/11}$ and $G\alpha_{i/o}$ (FR900359 and PTX 50 ng/mL overnight) reveals $G\alpha_s$-mediated cAMP production (**E, F**). [^{35}S]GTPγS binding is an integrated response with contribution from $G\alpha_{q/11}$ and $G\alpha_{i/o}$. Inhibition of $G\alpha_{q/11}$ (FR900359) singles out $G\alpha_{i/o}$-mediated [^{35}S]GTPγS binding (**H, I**). Data are shown as

mean ± s.e.m. of at least three independent experiments performed in triplicate (IP1 and cAMP) or quadruplicate ([^{35}S]GTPγS), and normalized as indicated.

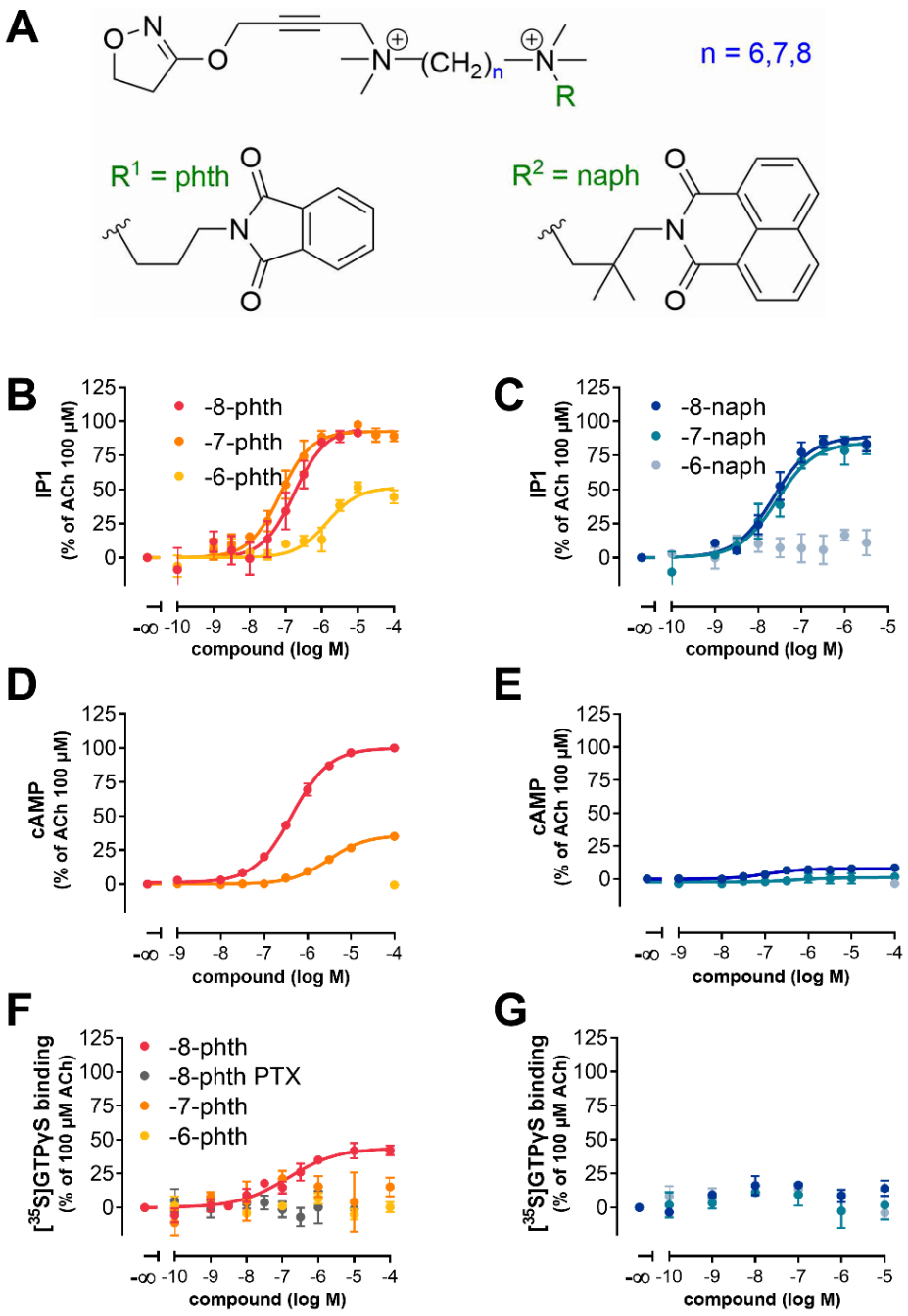

Figure 2: G protein-activation profiles of bitopic ligands strictly depend on linker length and type of allosteric moiety. (**A**) Molecular structures of bitopic ligands. (**B-G**) Concentration-response-curves of *phth*-derived (**B, D, F**) and *naph*-derived (**C, E, G**) bitopic ligands on activation of $G\alpha_{q/11}$ (IP1 accumulation) (**B, C**), $G\alpha_s$ (cAMP accumulation in the presence of PTX and

FR900359) (**D,** **E**), and $G\alpha_{i/o}$ ($[^{35}S]GTP\gamma S$ binding) (**F, G**). Data are shown as mean ± s.e.m. of at least three independent experiments performed in triplicate (IP1 and cAMP) or quadruplicate ($[^{35}S]GTP\gamma S$), and normalized as indicated.

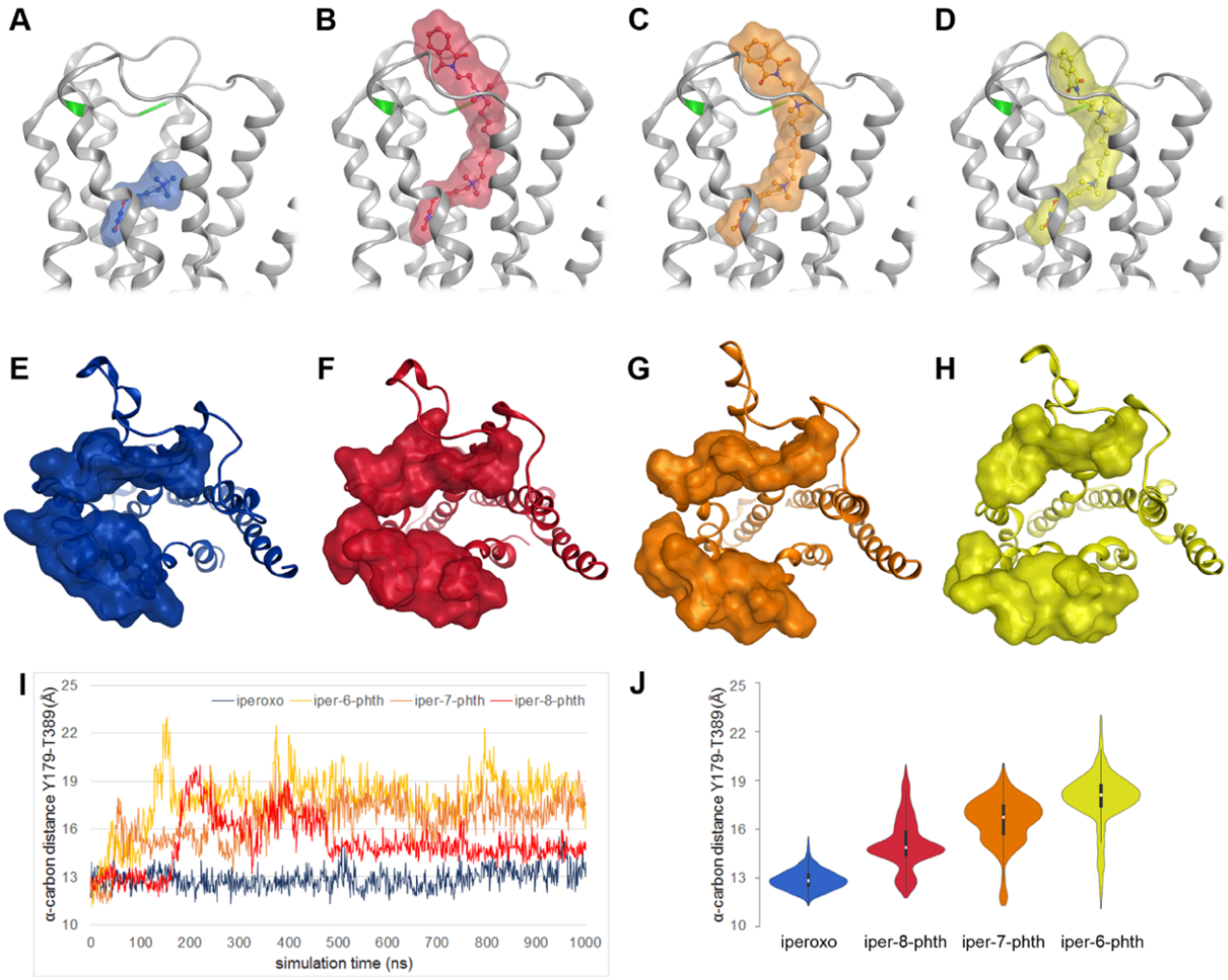

Figure 3: Bitopic ligands interfere with binding pocket closure upon M_1 receptor activation. (**A-D**) Binding modes of iperoxo (**A**), iper-8-phth (**B**), iper-7-phth (**C**) and iper-6-phth (**D**) derived from molecular docking to the active M_1 receptor model. Extracellular residues Y179 and T389 are shown as green ribbon. (**E-H**) Representative conformations from µs-MD simulations of M_1R in complex with iperoxo (**E**), iper-8-phth (**F**), iper-7-phth (**G**) and iper-6-phth (**H**) shown from the extracellular side. Parts of ECL2 and ECL3 are shown as surface to illustrate the size of the allosteric vestibule. (**I-J**) Alpha carbon distances between Y179 and T389 serve as a conformational descriptor for the closure of the binding pocket upon receptor activation, which is visualized as time-dependent distance plot (**I**) and violin plot (**J**).

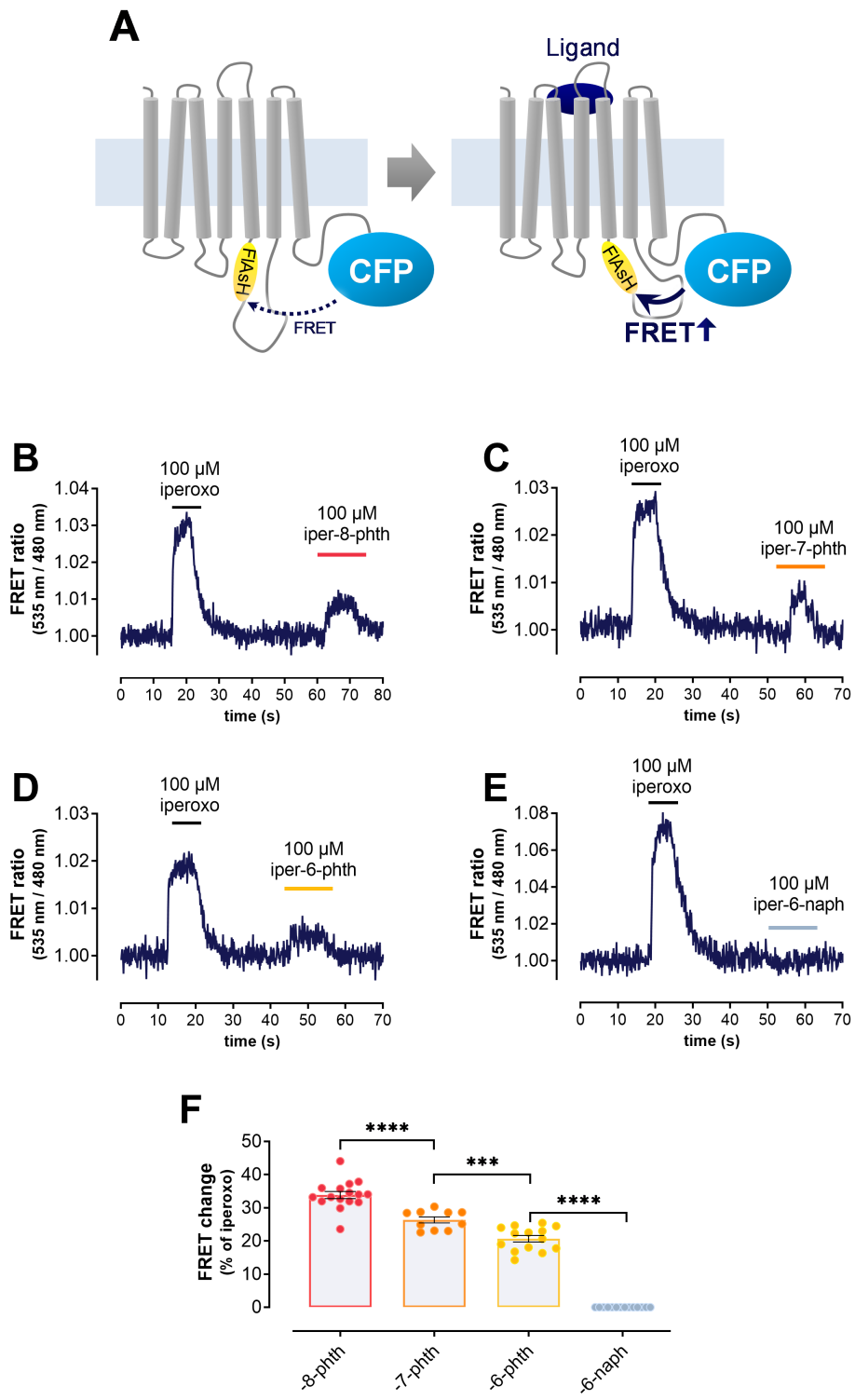

Figure 4: Bitopic ligands gradually alter intracellular conformational changes. (**A**) Schematic representation of the intracellular M_1R-FRET-sensor, depicting the FlAsH binding sequence in

ICL3 in yellow and the C-terminal CFP in cyan. (**B-E**) Corrected and normalized FRET ratios of single HEK293 cells stably expressing the M_1R-FRET-sensor. Cells were superfused with iperoxo and iper-8-ptht (**B**), iper-7-phth (**C**), iper-6-phth (**D**) and iper-6-naph (**E**). Shown are representative traces from one out of at least 3 independent single-cell experiments. (**F**) Bitopic ligand-induced FRET ratios pooled from all cells measured as in (**B-E**) were normalized to iperoxo. n=16 (iper-8-phth), 10 (iper-7-phth), 14 (iper-6-phth), and 14 (iper-6-naph) single cells. The columns represent means, the vertical bars s.e.m. ****P<0.0001, ***P<0.0005, one-way analysis of variance (ANOVA, Tukey's post-test).

FOR TABLE OF CONTENTS USE ONLY

Ligand-specific allosteric coupling controls G protein-coupled receptor signaling

Janine Holze[1,#], Marcel Bermudez[2,#], Eva Marie Pfeil[3], Michael Kauk[4], Theresa Bödefeld[1], Matthias Irmen[1], Carlo Matera[5], Clelia Dallanoce[5], Marco De Amici[5], Ulrike Holzgrabe[6], Gabriele Maria König[7], Christian Tränkle[1], Gerhard Wolber[2], Ramona Schrage[1], Klaus Mohr[1], Carsten Hoffmann[4], Evi Kostenis[3], and Andreas Bock[1,8]**

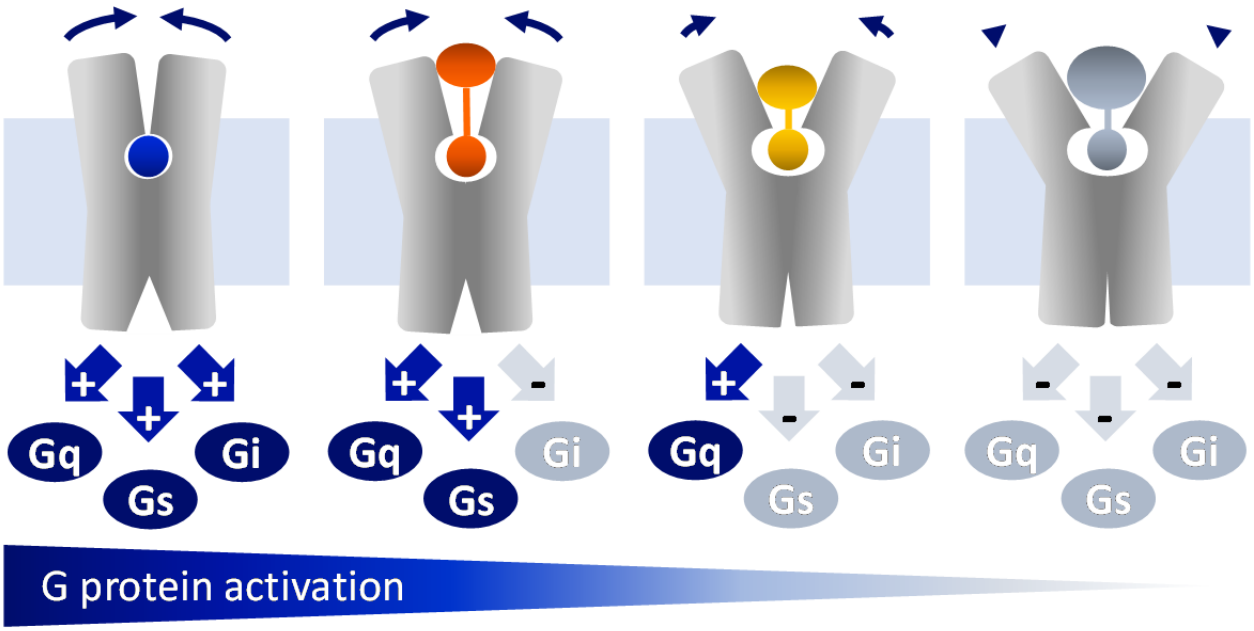

Synopsis:

At M_1 receptors, full agonists (blue) stabilize active receptor conformations that couple to multiple G-protein families ($G_{q/11}$, G_s, and $G_{i/o}$). Bitopic agonists that contain allosteric ligands covalently attached to orthosteric agonists by linkers of different lengths (orange and yellow) gradually hamper binding pocket closure (blue arrows) and, through allosteric coupling, progressively constrain activation of different G-protein families.